Nonlinear dynamics of a double bilipid membrane

C. Sample and A. A. Golovin
Department of Engineering Sciences and Applied Mathematics, Northwestern University, Evanston, Illinois 60208, USA
(Received 8 May 2007; revised manuscript received 3 August 2007; published 28 September 2007)

The nonlinear dynamics of a biological double membrane that consists of two coupled lipid bilayers, typical of some intracellular organelles such as mitochondria or nuclei, is studied. A phenomenological free-energy functional is formulated in which the curvatures of the two parts of the double membrane and the distance between them are coupled to the lipid chemical composition. The derived nonlinear evolution equations for the double-membrane dynamics are studied analytically and numerically. A linear stability analysis is performed, and the domains of parameters are found in which the double membrane is stable. For the parameter values corresponding to an unstable membrane, numerical simulations are performed that reveal various types of complex dynamics, including the formation of stationary, spatially periodic patterns.

DOI: 10.1103/PhysRevE.76.031925 PACS number(s): 87.16.Ac, 87.16.−b, 87.16.Dg

I. INTRODUCTION

Biological membranes are intricate structures composed of lipids, proteins, carbohydrates, and other materials that participate in a number of cell functions necessary to sustain life [1]. Some of the basic properties of biological membranes can be understood by studying the behavior of lipid bilayers; they represent the simplest model for complex biological membranes [2,3] and have been attracting great attention. Lipid bilayers are usually formed when amphiphilic molecules self-assemble and orient in water due to strong hydrophobic interactions. A fluid mosaic model of biological membranes, first introduced over thirty years ago, describes the molecular composition of a membrane as an asymmetric, fluid, lipidic bilayer [4].

In biomembranes, the three fundamental aspects of membrane phenomena include external degrees of freedom, such as membrane curvature, internal degrees of freedom, such as the local density of amphiphilic molecules and the local concentration of one of several types of amphiphiles, and the interaction between membranes [5]. The properties of a single-component, self-assembled membrane in equilibrium are, to a large extent, governed by the amount of energy needed to bend the bilayer [2]. Some models have been developed to introduce the local composition of a multicomponent bilayer in thermodynamic equilibrium [6–12]. It was shown, both theoretically and experimentally, that phase separation within a multicomponent membrane can lead to morphological transitions [8,9,13]. Bud formation is an example of such a change, in which a large "parent" vesicle sprouts out a spherical bud consisting of one of the lipid species [14,15].

In reality, biomembranes are constantly out of equilibrium as a result of the functioning of active components, i.e., proteins participating in ion transport, cell adhesion, locomotion, signaling, and other physiological processes. Diffusion of the active proteins in the membrane provides a nonthermal source of noise for membrane shape alterations. More realistic studies have recently included active proteins [16–20] or externally activated chemical processes [21,22] to model membranes as nonequilibrium systems that exhibit sustained time-dependent patterning.

So far, most of studies have been limited to single bilipid membranes. In nature, some intracellular organelles, such as mitochondria, nuclei, and chloroplasts, have two membranes, outer and inner ones [1], with an intermembrane region between them: the inner membrane separates the interior of the organelle from the intermembrane space and the latter is separated from the environment by the outer membrane.

The dynamics of such a double membrane has been much less studied theoretically. In fact, the only theoretical investigation of the dynamics of a double membrane that we are aware of is the one by Kats *et al.* [23]. They considered a model in which the free energy of a double-membrane system depends on the undulation (bending) deformations of the system as a whole and the squeezing deformations that depend on the modulations of the intermembrane distance. The effect of thermal fluctuations on the behavior of the two modes was investigated in [23] in the long-wave limit. It was shown that the behavior of the squeezing mode was strongly affected by its nonlinear coupling with the transverse hydrodynamic mode and that its characteristic frequency was independent of the bending elasticity.

In the present paper, we investigate the dynamics of a double bilayer membrane for the case when each of the two membranes consists of two different lipid components that can undergo phase separation. We focus on the effect of phase separation in the membranes on the morphology of the double-membrane system. We take into account the possible coupling between the intermembrane distance and the membrane compositions, as well as the composition dependence of the membrane spontaneous curvatures. In the present model, we do not consider nonequilibrium fluxes across the membranes and concentrate only on the relaxation of a double-membrane system toward thermodynamic equilibrium triggered by phase separation in one or both membranes. One of the main goals of our paper is to see whether the coupled dynamics of the two membranes in a double-membrane system can lead to the formation of complex structures.

II. THE MODEL

Consider two lipid bilayer membranes described as two-dimensional surfaces. We introduce a Cartesian coordinate

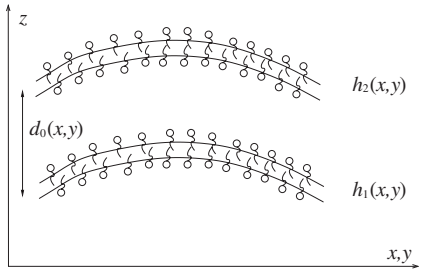

FIG. 1. Model setup.

system with the z axis normal to the flat membranes and in-plane coordinates $\mathbf{x}=(x,y)$. In the Monge parametrization [24], the two deformable surfaces are described by $z=h_1(x,y)$ and $z=h_2(x,y)$, respectively (see Fig. 1). Each membrane consists of two types of lipids, with the local composition characterized by an order parameter $\rho_{1,2}(x,y)$, where $\rho_{1,2}=0$ corresponds to a chemically homogeneous membrane. The spontaneous curvature of each membrane depends only on the corresponding order parameter, and the zero values of the order parameters correspond to flat membranes. We also assume that the double-membrane system is characterized by an equilibrium distance between the membranes that also depends on the order parameters $\rho_{1,2}$. We assume here that the double membrane undergoes relaxational dynamics toward thermodynamic equilibrium that can be described by means of an appropriate free-energy functional. Thus we ignore possible hydrodynamic effects associated with the incompressible fluid separating the two membranes, as well as possible hydrodynamic flows in the inner and outer regions. This assumption is reasonable in the case when the fluids surrounding the membranes are highly viscous and the membranes themselves are very permeable by the molecules of the fluids (see, e.g., [16]).

The free energy of the double-membrane system can be described by the following functional:

$$\mathcal{F}=\int\left(f_1(\rho_1)+\frac{\gamma_1}{2}|\nabla\rho_1|^2+f_2(\rho_2)+\frac{\gamma_2}{2}|\nabla\rho_2|^2+g(h_2-h_1,\rho_1,\rho_2)+\frac{\kappa_1}{2}(\nabla^2h_1-\eta_1\rho_1)^2+\frac{\kappa_2}{2}(\nabla^2h_2-\eta_2\rho_2)^2\right)dx\,dy. \quad (1)$$

Here the functions

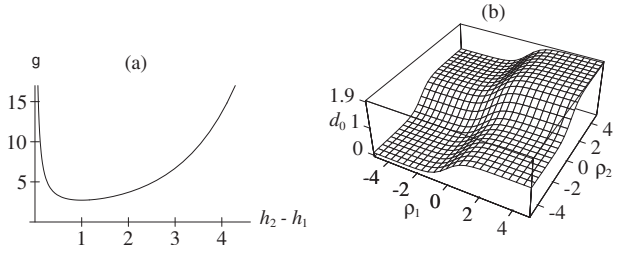

FIG. 2. (a) Intermembrane interaction potential $g(h_2-h_1,\rho_1,\rho_2)$ defined in (3); $\beta=1$, $d_0=1$, and $\lambda=1$. (b) Equilibrium intermembrane distance $d_0(\rho_1,\rho_2)$ defined in (4) where $d_{00}=1$ and $\Delta=0.9$.

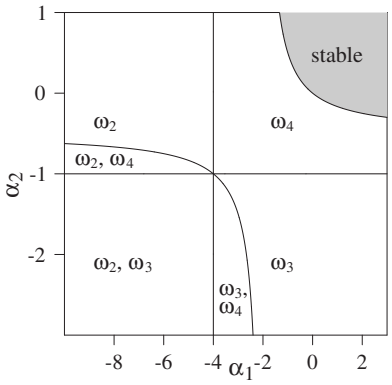

FIG. 3. Long-wave stability diagram in the (α_1,α_2) parameter plane. Modes indicated in each region are unstable in the long-wave limit. Here, $\lambda=0.1$, $\Delta=0.9$, $\beta=0.1$, $\kappa_1=1$, $\kappa_1=1$, $\kappa_2=1$, $\eta_1=2$, and $\eta_2=1$.

$$f_i(\rho_i)=\frac{\alpha_i}{2}\rho_i^2+\frac{\nu_i}{4}\rho_i^4,\quad i=1,2, \quad (2)$$

describe the chemical parts of the system free energy, the terms with coefficients $\kappa_{1,2}$ describe the bending rigidity of the two membranes, and the function g describes the energy penalty for the deviation of the intermembrane distance from its equilibrium value d_0. In order to be able to describe the nonlinear evolution of an unstable double membrane leading to large membrane deformations, and therefore not allowing the two membranes to cross each other, we assume the following intermembrane interaction potential:

$$g(h_2-h_1,\rho_1,\rho_2)=\beta\left(\frac{h_2-h_1}{d_0}\right)^{-\lambda}\exp\left(\frac{\lambda(h_2-h_1)}{d_0}\right), \quad (3)$$

where $\lambda>0$ describes the strong repulsion of the two membranes when they approach each other so that the intermembrane distance becomes much smaller than the equilibrium distance d_0 corresponding to the minimum of this function. The function (3) is shown in Fig. 2(a). Obviously, this potential is not relevant when the distance between the two membranes becomes very large, since at very large distances the membrane interaction should decay; however, we are not interested in this case in the present paper.

The equilibrium distance d_0 is assumed to be dependent on the order parameters $\rho_{1,2}$. If each of the two membranes can be composed of two components A and B, four cases of "pure" membrane compositions should be considered: (A,A), (A,B), (B,A), and (B,B). Clearly, the equilibrium intermembrane distance in the cases (A,B) and (B,A) must be the same, whereas in the cases (A,A) and (B,B) it can be different. The function

$$d_0(\rho_1,\rho_2)=d_{00}+\frac{\Delta}{2}(\tanh\rho_1+\tanh\rho_2) \quad (4)$$

has the required property, as shown in Fig. 2(b).

The terms $(\gamma_1/2)|\nabla\rho_1|^2$ and $(\gamma_2/2)|\nabla\rho_2|^2$ in (1) correspond to the energies of the boundaries between the domains with different chemical compositions within each membrane. Thus, the first four terms of the energy functional correspond

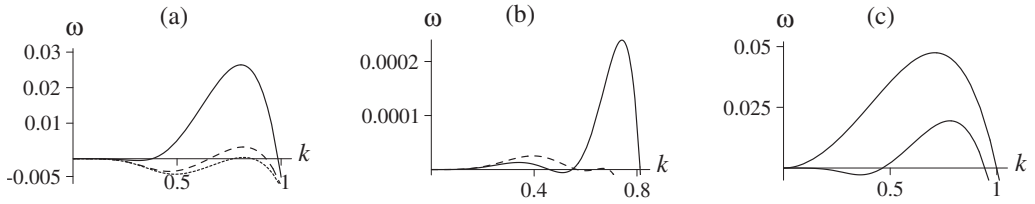

FIG. 4. Examples of dispersion curves determined by (16) with $\alpha_1=-1$ and $\kappa_2=1$ as common parameters. (a) One unstable short-wave mode where $\alpha_2=1$, $\kappa_1=2$, $\eta_2=1$, $\eta_1=$ (solid line) 2, (dashed line) 3.5, and (dotted line) 4. (b) One unstable long- and short-wave mode where $\alpha_2=1$, $\kappa_1=1$, solid line $\eta_1=4.75$, $\eta_2=5$, and dashed line $\eta_1=5.05$, $\eta_2=5.5$. (c) Two monotonically unstable (one long-wave, one short-wave) modes where $\alpha_2=-1$, $\kappa_1=0.2$, $\eta_1=2$, and $\eta_2=2$.

to the typical Ginzburg-Landau free energy for a phase separating system. The terms with local extrinsic curvatures that, from the Monge parametrization, are approximated as $\nabla^2 h_{1,2}$ are well known as the Helfrich Hamiltonian [24,25]. Note that the surface tension contribution can be neglected in the free energy for self-assembled free membranes [23]. All the parameters are positive except for $\alpha_{1,2}$, $\delta_{1,2}$, and $\eta_{1,2}$, which can have either sign. Note also that in a real system, such as the double membranes in mitochondria, the chemical part of the free-energy functional of the two membranes can be much more complicated and may involve several order parameters for each membrane. Here we focus on the simplest possible case when each membrane is characterized by one order parameter, as a means to understand possible qualitative effects of the coupling between the membrane chemical composition and its morphology. The dynamics of a multicomponent single bilipid membrane has recently been studied in [26,27].

The evolution of the order parameters ρ_1 and ρ_2 is described by the conservation dynamics,

$$\partial_t \rho_{1,2} + \nabla \cdot j_{1,2} = 0, \tag{5}$$

where the fluxes $j_{1,2}$ can be expressed through the corresponding chemical potentials $\mu_{1,2}$ as

$$j_1 = -D_1 \nabla \mu_1 - D_{12} \nabla \mu_2, \tag{6}$$

$$j_2 = -D_2 \nabla \mu_2 - D_{21} \nabla \mu_1. \tag{7}$$

Here $D_{1,2}$, D_{12}, and D_{21} are the elements of the kinetic coefficient matrix, and $D_{12}=D_{21}$, according to the Onsager principle [28]. Since $\mu_{1,2}=\delta\mathcal{F}/\delta\rho_{1,2}$, we obtain the following evolution equations for the order parameters:

$$\frac{\partial \rho_1}{\partial t} = D_1 \nabla^2 \left(\frac{\delta \mathcal{F}}{\delta \rho_1} \right) + D_{12} \nabla^2 \left(\frac{\delta \mathcal{F}}{\delta \rho_2} \right), \tag{8}$$

$$\frac{\partial \rho_2}{\partial t} = D_2 \nabla^2 \left(\frac{\delta \mathcal{F}}{\delta \rho_2} \right) + D_{12} \nabla^2 \left(\frac{\delta \mathcal{F}}{\delta \rho_1} \right). \tag{9}$$

Thus, the coefficients $D_{1,2}$ describe the diffusion of the order parameter within the corresponding membrane, and the

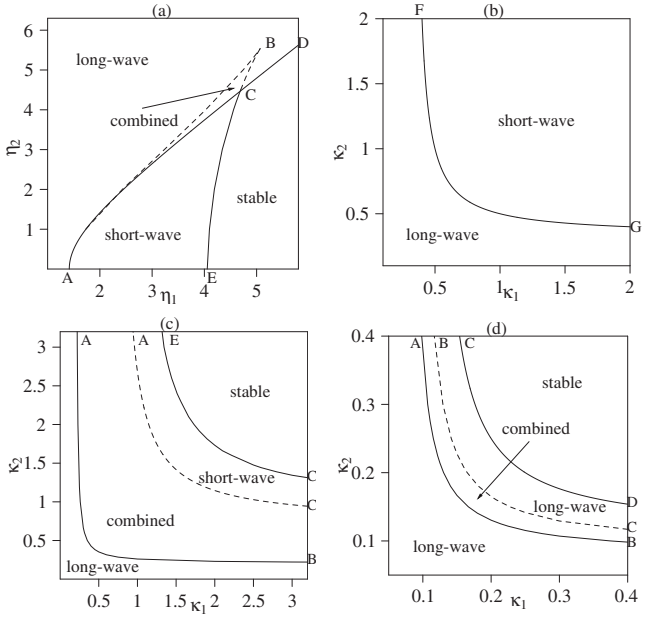

FIG. 5. Neutral stability curves for the case of zero or one unstable mode with parameter values $\alpha_1=-1$, $\alpha_2=1$, (a) $\kappa_1=1$, $\kappa_2=1$, (b) $\eta_1=2$, $\eta_2=1$, (c) $\eta_1=4.65$, $\eta_2=4.5$, and (d) $\eta_1=5$, $\eta_2=4$.

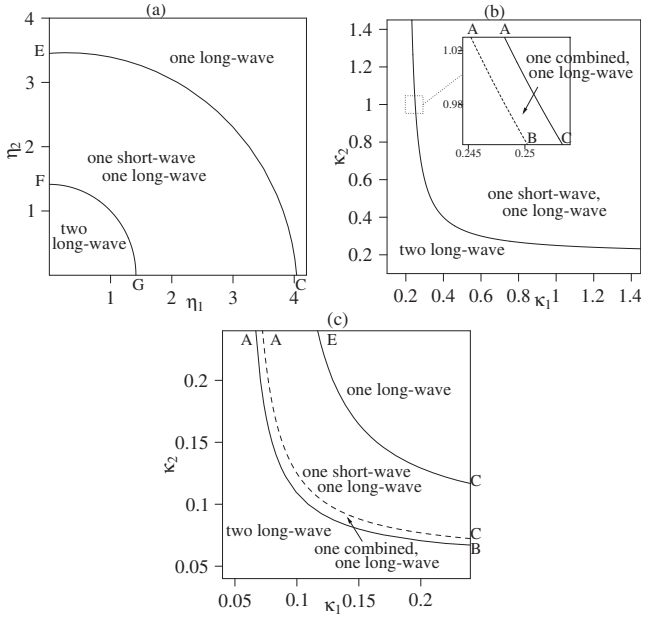

FIG. 6. Neutral stability curves for the case of one or two unstable modes with parameter values $\alpha_1=-1$, $\alpha_2=-1$, (a) $\kappa_1=1$, $\kappa_2=1$, (b) $\eta_1=2$, $\eta_2=1$, and (c) $\eta_1=3$, $\eta_2=3$.

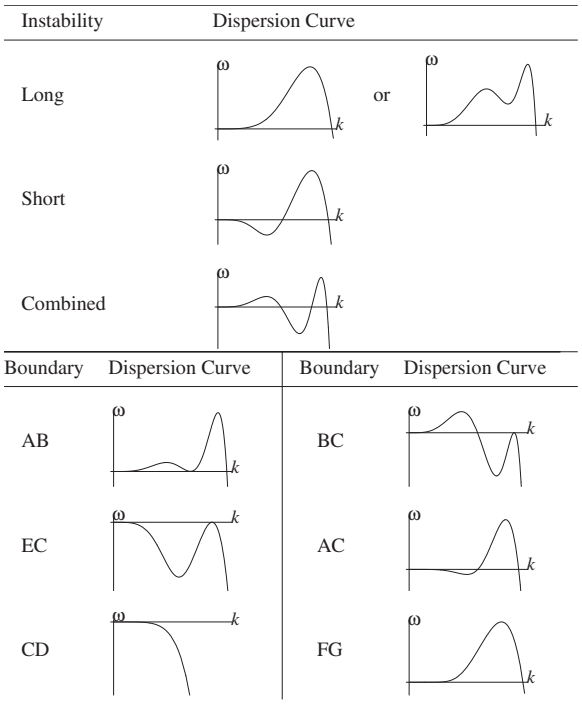

FIG. 7. Types of instabilities and the corresponding dispersion curves for the regions and boundaries in Figs. 5 and 6.

coefficient D_{12} describes the possibility of inducing a diffusion flux in one of the membranes by the order-parameter gradient in the other membrane. The cross-diffusion effect should depend on the distance between the two membranes. One can expect it to be significant if the intermembrane distance is of the same order of magnitude as or smaller than the typical radius of intermolecular forces acting between the two lipid bilayers. Otherwise, the cross-diffusion effect is expected to be negligible. Although we are not aware of any measurements of cross-diffusion effect in double membranes, we keep it in our analysis for the sake of generality. Of course, our results are also valid for the case $D_{12}=0$. We will in future refer to the coefficients D as diffusion coefficients.

The membrane shapes are described by the relaxational dynamics

$$\frac{\partial h_1}{\partial t} = -M_1 \frac{\delta \mathcal{F}}{\delta h_1}, \tag{10}$$

$$\frac{\partial h_2}{\partial t} = -M_2 \frac{\delta \mathcal{F}}{\delta h_2}, \tag{11}$$

where $M_{1,2}$ are the mobility parameters. Thus, after changing $h_2 - d_{00} \to h_2$, the membrane dynamics is described by the following system of equations:

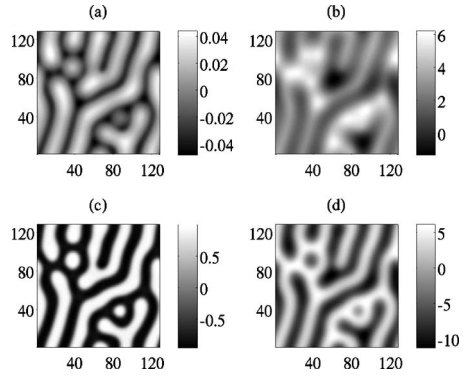

FIG. 8. Numerical solution of the system (12)–(15) at a particular moment of time for the case when the second mode is long-wave unstable: (a) $\rho_2(x,y)$, (b) $h_2(x,y)$, (c) $\rho_1(x,y)$, and (d) $h_1(x,y)$. Here the parameter values are $\alpha_1=-1$, $\alpha_2=1$, $\kappa_1=0.9$, $\kappa_2=1$, $\eta_1=1$, and $\eta_2=0.1$.

$$\begin{aligned}\frac{\partial \rho_1}{\partial t} &= D_1[(\alpha_1 + \eta_1^2\kappa_1)\nabla^2\rho_1 - \gamma_1\nabla^4\rho_1 - \eta_1\kappa_1\nabla^4 h_1] \\ &+ D_1\nabla^2\left[\nu_1\rho_1^3 + \frac{\Delta}{2}\lambda g(h_2 - h_1, \rho_1, \rho_2) \right. \\ &\left. \times\left(\frac{1}{d_0} - \frac{h_2 - h_1}{d_0^2}\right)\mathrm{sech}^2\,\rho_1\right] + D_{12}[(\alpha_2 + \eta_2^2\kappa_2)\nabla^2\rho_2 \\ &- \gamma_2\nabla^4\rho_2 - \eta_2\kappa_2\nabla^4 h_2] \\ &+ D_{12}\nabla^2\left[\nu_2\rho_2^3 + \frac{\Delta}{2}\lambda g(h_2 - h_1, \rho_1, \rho_2) \right. \\ &\left. \times\left(\frac{1}{d_0} - \frac{h_2 - h_1}{d_0^2}\right)\mathrm{sech}^2\,\rho_2\right],\end{aligned} \tag{12}$$

$$\begin{aligned}\frac{\partial \rho_2}{\partial t} &= D_2[(\alpha_2 + \eta_2^2\kappa_2)\nabla^2\rho_2 - \gamma_2\nabla^4\rho_2 - \eta_2\kappa_2\nabla^4 h_2] \\ &+ D_2\nabla^2\left[\nu_2\rho_2^3 + \frac{\Delta}{2}\lambda g(h_2 - h_1, \rho_1, \rho_2) \right. \\ &\left. \times\left(\frac{1}{d_0} - \frac{h_2 - h_1}{d_0^2}\right)\mathrm{sech}^2\,\rho_2\right] + D_{12}[(\alpha_1 + \eta_1^2\kappa_1)\nabla^2\rho_1 \\ &- \gamma_1\nabla^4\rho_1 - \eta_1\kappa_1\nabla^4 h_1] + D_{12}\nabla^2\left[\nu_1\rho_1^3 + \frac{\Delta}{2}\lambda g(h_2 \right. \\ &\left. - h_1, \rho_1, \rho_2)\left(\frac{1}{d_0} - \frac{h_2 - h_1}{d_0^2}\right)\mathrm{sech}^2\,\rho_1\right],\end{aligned} \tag{13}$$

$$\begin{aligned}\frac{\partial h_1}{\partial t} &= M_1\left[\eta_1\kappa_1\nabla^2\rho_1 - \kappa_1\nabla^4 h_1 - \lambda g(h_2 - h_1, \rho_1, \rho_2) \right. \\ &\left. \times\left(\frac{1}{h_2 - h_1} - \frac{1}{d_0}\right)\right],\end{aligned} \tag{14}$$

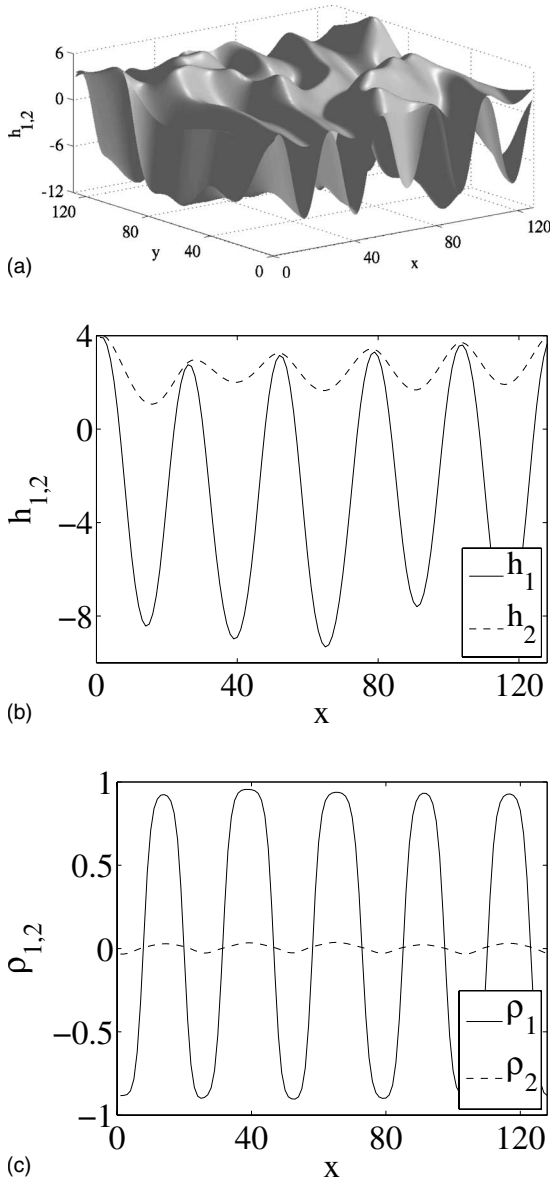

FIG. 9. (a) Surface plot and (b) cross section of the shape and (c) composition of the membranes in Fig. 8.

$$\frac{\partial h_2}{\partial t} = M_2\left[\eta_2\kappa_2\nabla^2\rho_2 - \kappa_2\nabla^4 h_2 + \lambda g(h_2 - h_1, \rho_1, \rho_2) \times\left(\frac{1}{h_2 - h_1} - \frac{1}{d_0}\right)\right]. \tag{15}$$

III. LINEAR STABILITY ANALYSIS

In this section we perform a linear stability analysis of the planar double-membrane described by Eqs. (12)–(15) in order to understand under which conditions such a membrane is stable. The steady state corresponds to planar, chemically homogeneous membranes, $h_1=0$, $h_2=d_{00}$, $\rho_1=\rho_2=0$.

Consider infinitesimal perturbations of the steady state, $\tilde{\rho}_{1,2}=R_{1,2}e^{i\mathbf{k}\cdot\mathbf{x}+\omega t}$ and $\tilde{h}_{1,2}=H_{1,2}e^{i\mathbf{k}\cdot\mathbf{x}+\omega t}$, and linearize the system (12)–(15) to obtain the following dispersion relation:

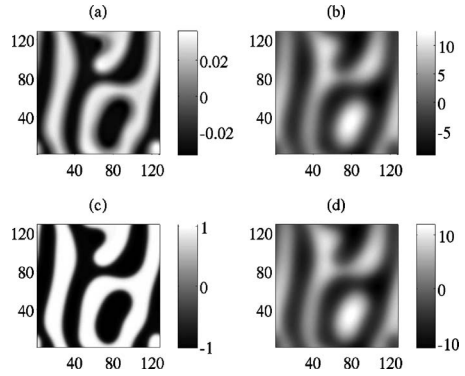

FIG. 10. Numerical solution of the system (12)–(15) at a particular moment in time for the case when the fourth mode is long-wave unstable: (a) $\rho_2(x,y)$, (b) $h_2(x,y)$, (c) $\rho_1(x,y)$, and (d) $h_1(x,y)$. Here the parameter values are $\alpha_1=-1$, $\alpha_2=1$, $\kappa_1=12$, $\kappa_2=1$, $\eta_1=0.3$, and $\eta_2=10$.

$$\omega^4 + A(k)\omega^3 + B(k)\omega^2 + C(k)\omega + D(k) = 0, \tag{16}$$

where

$$A(k) = a_0 + a_2k^2 + a_4k^4, \tag{17}$$

$$B(k) = b_2k^2 + b_4k^4 + b_6k^6 + b_8k^8, \tag{18}$$

$$C(k) = c_4k^4 + c_6k^6 + c_8k^8 + c_{10}k^{10} + c_{12}k^{12}, \tag{19}$$

$$D(k) = d_8k^8 + d_{10}k^{10} + d_{12}k^{12} + d_{14}k^{14} + d_{16}k^{16}, \tag{20}$$

and the coefficients depend on physical parameters (and are given in the Appendix). For $k=0$, Eq. (16) has three zero roots corresponding to three zero modes: uniform translation of the whole system and conservation of the order parameters in the two membranes. The nonzero mode $\omega_1=-a_0$ corresponds to a change of the intermembrane distance. For $k\neq 0$, it corresponds to the varicose deformation mode.

The membrane is stable if all roots of Eq. (16) have negative real parts. A necessary and sufficient condition is given by the Routh-Hurwitz criterion [29]. We find that the necessary condition for stability that gives the short-wave cutoff is

$$D_1D_2 - D_{12}^2 > 0. \tag{21}$$

For $k\ll 1$, we expand the varicose deformation mode $\omega_1=\omega_1^{(0)}+\omega_1^{(2)}k^2$, the two phase separation modes $\omega_{2,3}=\omega_{2,3}^{(2)}k^2+\omega_{2,3}^{(4)}k^4$, and the mixed mode associated with the coupling between bending rigidity of the membranes and their chemical composition, $\omega_4=\omega_4^{(4)}k^4$, where, provided $(\alpha_1+\eta_1^2\kappa_1)(\alpha_2+\eta_2^2\kappa_2)\neq 0$,

$$\omega_1^{(0)} = -a_0 = -\lambda\beta e^{\lambda}(M_1 + M_2),$$

$$\omega_1^{(2)} = -a_2 + \frac{b_2}{a_0} = -\frac{1}{4}\lambda\beta e^{\lambda}\Delta^2(D_1 + D_2 + 2D_{12}),$$

$$\omega_{2,3}^{(2)} = -\frac{b_2 \pm \sqrt{b_2^2 - 4a_0c_4}}{2a_0},$$

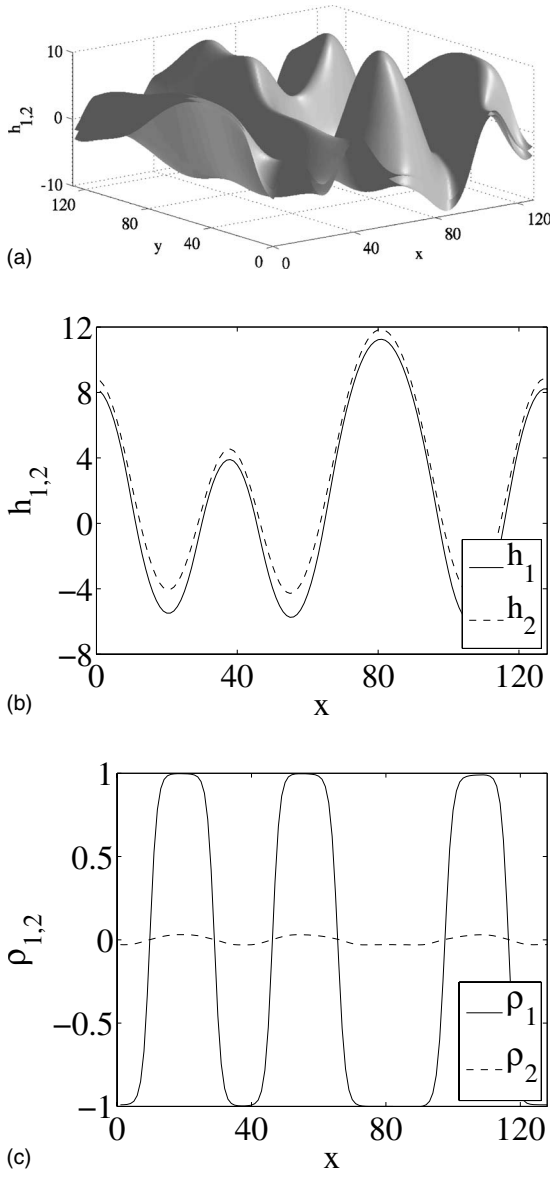

FIG. 11. (a) Surface plot and (b) cross section of the shape and (c) composition of the membranes in Fig. 10.

$$\omega_{2,3}^{(4)} = -\frac{d_8 + w_{2,3}^{(2)}\{c_6 + w_{2,3}^{(2)}[b_4 + w_{2,3}^{(2)}(a_2 + w_{2,3}^{(2)})]\}}{c_4 + w_{2,3}^{(2)}(2b_2 + 3a_0 w_{2,3}^{(2)})},$$

$$\omega_4^{(4)} = -\frac{d_8}{c_4} = -\frac{M_1 M_2[\alpha_1\alpha_2(\kappa_1+\kappa_2) + \kappa_1\kappa_2(\alpha_2\eta_1^2 + \alpha_1\eta_2^2)]}{(M_1+M_2)(\alpha_1+\eta_1^2\kappa_1)(\alpha_2+\eta_2^2\kappa_2)}, \tag{22}$$

with the coefficients given in the Appendix. In this expansion, provided the condition (21) is satisfied, ω_1 is always negative, and the long-wave varicose mode is damped. If $(\alpha_1+\eta_1^2\kappa_1)=0$ or $(\alpha_2+\eta_2^2\kappa_2)=0$, we obtain $\omega_2=\omega_2^{(2)}k^2+\omega_2^{(4)}k^4$ and $\omega_{3,4}=\omega_{3,4}^{(3)}k^3+\omega_{3,4}^{(4)}k^4$, where $\omega_2^{(2)}$ and $\omega_2^{(4)}$ remain the same as in Eqs. (22) and

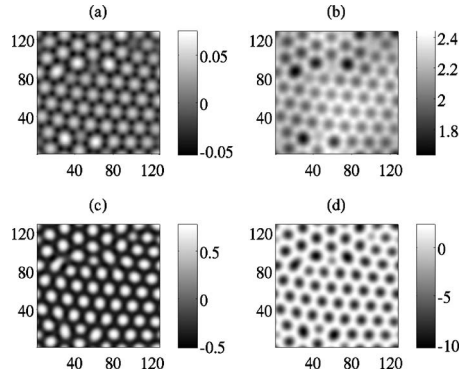

FIG. 12. Numerical solution of the system (12)–(15) at a particular moment of time for the case when the fourth mode is short-wave unstable: (a) $\rho_2(x,y)$, (b) $h_2(x,y)$, (c) $\rho_1(x,y)$, and (d) $h_1(x,y)$. Here the parameter values are $\alpha_1=-1$, $\alpha_2=1$, $\kappa_1=2$, $\kappa_2=1$, $\eta_1=4$, and $\eta_2=1$.

$$\omega_{3,4}^{(3)} = \pm\sqrt{\frac{-d_8}{b_2}}, \quad \omega_{3,4}^{(4)} = \frac{a_0 d_8 - b_2 c_6}{2b_2^2}. \tag{23}$$

For the case when $\alpha_1+\eta_1^2\kappa_1=\alpha_2+\eta_2^2\kappa_2=0$, one obtains $\omega_{2,3}=\omega_{2,3}^{(3)}k^3+\omega_{2,3}^{(4)}k^4$ and $\omega_4=\omega_4^{(4)}k^4$, where

$$\omega_{2,3}^{(3)} = \pm\sqrt{\frac{-c_6}{a_0}}, \quad \omega_{2,3}^{(4)} = \frac{1}{2}\left(\frac{d_{10}}{c_6} - \frac{b_4}{a_0}\right), \quad \omega_4^{(4)} = -\frac{d_{10}}{c_6}. \tag{24}$$

Using the Routh-Hurwitz criterion, we conclude that the system is always stable for α_1 and α_2 positive, the system may become unstable when either α_1 or α_2 is negative, and the system is always unstable for both α_1 and α_2 negative, with at most two unstable modes. In the long-wave limit, the necessary and sufficient conditions for the stability of the second, third, and fourth modes are

$$\alpha_1 + \eta_1^2\kappa_1 > 0, \tag{25}$$

$$\alpha_2 + \eta_2^2\kappa_2 > 0, \tag{26}$$

$$\frac{\alpha_1\alpha_2(\kappa_1+\kappa_2) + \kappa_1\kappa_2(ha_2\eta_1^2 + \alpha_1\eta_2^2)}{(\alpha_1+\eta_1^2\kappa_1)(\alpha_2+\eta_2^2\kappa_2)} > 0, \tag{27}$$

respectively. If (27) holds and either or both (25) and (26) hold, the fourth mode may become unstable with respect to perturbations with finite wavelength (provided α_1 or α_2 is negative). Otherwise, if α_1 and α_2 are negative and (25) and (26) hold, one mode may become unstable with respect to perturbations with finite wavelength. Figure 3 shows examples of regions in the (α_1, α_2) parameter plane in which different modes are subject to long-wave instability. Note that, due to the coupling between the intermembrane distance and the chemical compositions of the two membranes, phase separation in only one of the membranes [i.e., when one of the conditions (25) and (26) is not satisfied] can cause morphological instability in the whole double-membrane system. This situation is in a sense analogous to instability of a single membrane when phase separation of a mixed state causes the

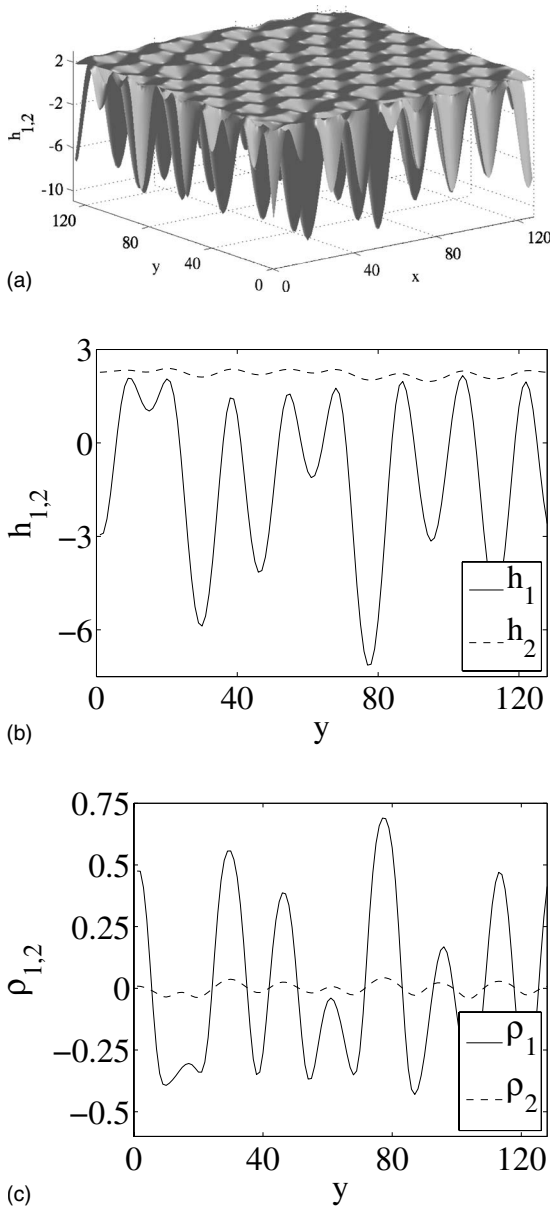

FIG. 13. (a) Surface plot and (b) cross section of the shape and (c) composition of the membranes in Fig. 12.

instability of a flat membrane due to the coupling between the chemical composition and the membrane curvature [9]. Similarly, as in the case of a single membrane [21], the double-membrane instability is triggered by phase separation only and cannot occur simply due to the coupling between the chemical composition and the curvature. Indeed, in the absence of phase separation, i.e., for $\alpha_{1,2}>0$, the basic state of two flat, chemically homogeneous membranes corresponds to a minimum point of the free-energy functional and therefore is absolutely stable. Conversely, when $\alpha_1<0$ or $\alpha_2<0$, the basic state can become a saddle point, which leads to the instability.

The most interesting examples of dispersion curves are shown in Fig. 4: one can see that the system can have one unstable short-wave mode [Fig. 4(a)], one unstable mode that corresponds to both long- and short-wave instability

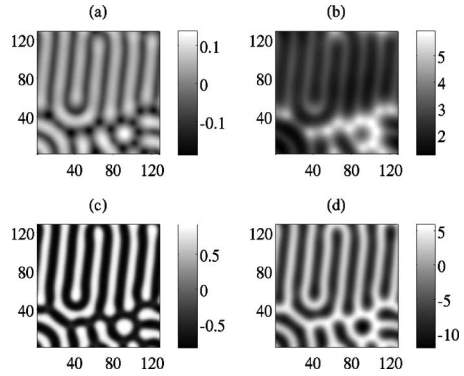

FIG. 14. Numerical solution of the system (12)–(15) at a particular moment of time for the case when the fourth mode is short-wave unstable: (a) $\rho_2(x,y)$, (b) $h_2(x,y)$, (c) $\rho_1(x,y)$, and (d) $h_1(x,y)$. Here the parameter values are $\alpha_1=-1$, $\alpha_2=1$, $\kappa_1=2$, $\kappa_2=1$, $\eta_1=2$, and $\eta_2=1$.

[Fig. 4(b)], and also one long-wave and one short-wave mode [Fig. 4(c)] present at the same time. Here and throughout the rest of the paper, $D_1=D_2=M_1=M_2=\gamma_1=\gamma_2=1$, $D_{12}=0$, $\lambda=0.1$, $\beta=0.1$, and $\Delta=0.9$.

Examples of neutral stability diagrams in the parameter planes corresponding to the bending rigidities and the coupling constants describing the effect of the membrane composition on the spontaneous curvatures are shown in Figs. 5 and 6. Figure 5 corresponds to the case when only one mode can be unstable. This mode can be long wave, short wave, or "combined" as shown in Fig. 7. An example of the neutral stability boundaries in the case when two modes can become unstable is shown in Fig. 6. Here also the two modes can be both long wave, one long wave and one short wave, or combined (see also Fig. 7).

IV. NUMERICAL SIMULATIONS

In this section, we describe the results of the numerical simulations of the system (12)–(15). We have represented the system (12)–(15) in the form $\mathbf{u}_t=L\mathbf{u}+(N-L)\mathbf{u}$, where $\mathbf{u}=(\rho_1,h_1,\rho_2,h_2)^T$, N is the right-hand side of (12)–(15), and L is N linearized around the steady state corresponding to $h_1=0$, $h_2=d_{00}$, $\rho_1=0$, and $\rho_2=0$. Numerical integration has been performed using a pseudospectral method, with time integration in Fourier space, using the Crank-Nicolson scheme for the linear operator L and the Adams-Bashforth scheme for the nonlinear operator $N-L$. We use periodic boundary conditions and the initial conditions corresponding to small-amplitude random perturbations of the steady state. Two-dimensional numerical simulations have been performed for the cases with one or two unstable modes that are long wave, short wave, or combined (see Fig. 7). In the figures below, the representative cases are shown.

Figures 8 and 9 show the membrane shapes and the corresponding order parameters in the case when the system is unstable with respect to one of the two long-wave phase separation modes, ω_2 or ω_3. We observe that in this case, for $\omega_2>0$ ($\omega_3>0$), the first (second) membrane develops deep

grooves that follow the corresponding phase separation process, while the second (first) membrane develops shallow grooves coupled to small changes in the corresponding order parameter (see Figs. 8 and 9). Note that deep grooves in the first (inner) membrane can be thought of as the precursors to the formation of cristae in mitochondria.

Figures 10 and 11 show the shapes of the two membranes and the order parameters for the case when the mixed long-wave mode ω_4 is unstable. One can see that in this case the two membranes develop labyrinth-type structures coupled to the order-parameter fields. The corrugations of the two membranes are in phase, and the membrane deformations are much larger than the distance between the membranes (see Figs. 10 and 11). Note also that, in this particular case, the variations of the order parameter in the second membrane are much smaller than those in the first one; this is because phase separation occurs in the first membrane ($\alpha_1 < 0$), while the order-parameter variations in the second membrane are slaved to those in the first one and are smeared out by diffusion ($\alpha_2 > 0$).

The most interesting feature of the coupled dynamics of the two membranes is that the mixed mode ω_4, as shown in the previous section, can exhibit short-wave instability and therefore lead to pattern formation. The results of numerical simulations corresponding to this interesting case are shown in Figs. 12 and 13. One can see the shapes of the two membranes forming hexagonal patterns. The membrane shapes are correlated with the order-parameter field (chemical composition) due to the coupling between the latter and the spontaneous curvature. In the case shown in Figs. 12 and 13 the amplitude of the pattern in the first membrane is much larger than that in the second one since $\alpha_1 = -1$ and $\alpha_2 = 1$, and the phase separation occurs primarily in the first membrane.

Note that the short-wave instability occurs when certain parameters exceed their critical values. In the case shown in Figs. 12 and 13, we chose the bifurcation parameter to be the spontaneous curvature coefficient of the first membrane, η_1. With the decrease of η_1 the system becomes more unstable. The patterns shown in Figs. 12 and 13 correspond to $\eta_1 = 4$. With the increase of supercriticality (decrease of η_1) the symmetry of the pattern changes: the hexagonal pattern becomes unstable with respect to the stripe pattern. Such stripe patterns formed in the membranes at $\eta_1 = 2$ are shown in Figs. 14 and 15. Note that the transition from a hexagonal to a stripe pattern with the increase of supercriticality is a typical phenomenon in pattern formation [30].

We also note that, in [21], a Turing-type instability in a *single* bilipid biological membrane was shown to occur in the case when there are chemical reactions between different types of lipids. This also can result in the formation of spatially regular hexagonal or stripe patterns [21]. In our case, the Turing-type instability and pattern formation result from the coupling between the two bilipid membranes.

We have also run numerical simulations for the case when there is one unstable mode ω_4 that has two unstable domains corresponding to long and short waves [see Fig. 4(b)]. In this case we have observed that, when the growth rate corresponding to the short-wave instability is larger than that corresponding to the long-wave one, a hexagonal pattern is formed (see Fig. 16). In the case when the long-wave part of the dispersion curve has the higher growth rate, a labyrinth pattern develops, similar to the one shown in Fig. 10.

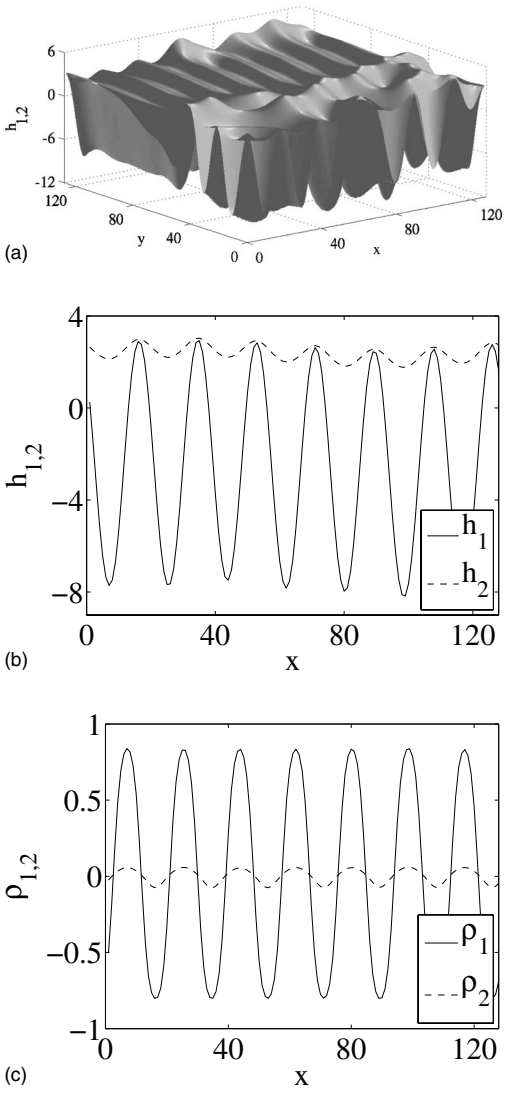

FIG. 15. (a) Surface plot and (b) cross section of the shape and (c) composition of the membranes in Fig. 14.

Finally, we have also performed numerical simulations for the case when there are two unstable modes, either both long wave or one long (ω_2 or ω_3) and one short wave (ω_4). In all the cases, the membrane shapes are observed to be in phase and to exhibit a dominant phase separation process, so that the membrane shape and the order-parameter field look similar to those shown in Fig. 10. The pattern evolution in time has been found to exhibit coarsening typical of phase separating systems: the characteristic scale of surface structures and the amplitude of the membrane corrugations grow with time.

V. CONCLUSIONS

In conclusion, we have proposed a model for the phase separation dynamics of a double lipid bilayer membrane. Such double membranes are typical of some intracellular or-

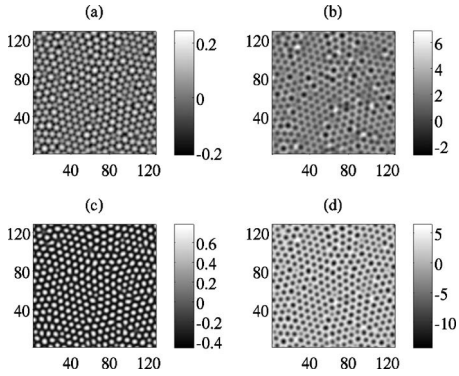

FIG. 16. Numerical solution of the system (12)–(15) at a particular moment of time for the case when the fourth mode has a combined instability: (a) $\rho_2(x,y)$, (b) $h_2(x,y)$, (c) $\rho_1(x,y)$, and (d) $h_1(x,y)$. Here the parameter values are $\alpha_1=-1$, $\alpha_2=1$, $\kappa_1=1$, $\kappa_2=1$, $\eta_1=4.75$, and $\eta_2=5$.

ganelles such as mitochondria or nuclei. Our model describes relaxation of the membrane shapes (spontaneous curvatures) and the intermembrane distance toward thermodynamic equilibrium induced by phase separation in one or both of the membranes. The key ingredient of our model is the coupling of the membrane shapes and the intermembrane distance to the membranes' chemical composition.

Within the framework of this model, we have performed a linear stability analysis and found the conditions under which such a double membrane is stable. System instability can be caused by phase separation in one of the membranes which, due to the coupling between the membrane geometry and the chemical composition, leads to morphological changes in the two membranes. We have found that there are two types of instabilities. One type is the long-wave instability, which is associated with phase separation in one of the membranes and leads to the formation of labyrinth-type morphological structures in both membranes that coarsen in time. The other type is the short-wave instability, which is caused by the coupling between the two membranes. Near threshold, this instability results in the formation of spatially regular hexagonal morphological structures. Farther from the instability threshold, the system exhibits a transition from hexagonal to striped structures, typical of many other pattern forming systems. Also, we have observed that, with the formation of such morphological structures, it is possible that, due to asymmetry of the properties of the two membranes, the amplitude of the shape corrugations of one membrane will be much larger than that of the other one. This can be considered as a precursor to the formation of such structures as cristae in mitochondria.

Thus, we have shown that phase separation in a double-membrane system can lead to the formation of complex spatial morphological structures. Of course, our present model is far from being able to describe a real biological membrane as in mitochondria or nuclei. A model describing a realistic double-membrane system must include, first of all, nonequilibrium chemical fluxes across the two membranes, into and out of the intermembrane space. Also, hydrodynamic flows generated in the intermembrane space as well as in the inner and outer regions can be important, especially for mitochondria because of the low permeability of the inner membrane. Yet another important factor is the presence of multiple chemical components in the two membranes which can require a description by means of several order parameters. We plan to include the above effects in further development of our model of a double-membrane system that will be presented elsewhere.

ACKNOWLEDGMENTS

This work was supported by the U.S. DOE Grant No. DE-FG02-03ER46069. C.S. also acknowledges the support of the NSF-IGERT. Part of this work was done during the visit of C.S. to Professor M. Toner's laboratory at Harvard Medical School. We thank Professor Toner for his hospitality and stimulating discussions.

APPENDIX

The coefficients in Eqs. (17)–(20) are

$$a_0 = e^{\lambda}\beta\lambda(M_1+M_2),$$

$$a_2 = \frac{1}{4}[2e^{\lambda}\beta\lambda D_{12}\Delta^2 + D_1(e^{\lambda}\beta\lambda\Delta^2 + 4\alpha_1 + 4\eta_1^2\kappa_1) + D_2(e^{\lambda}\beta\lambda\Delta^2 + 4\alpha_2 + 4\eta_2^2\kappa_2)],$$

$$a_4 = D_1\gamma_1 + D_2\gamma_2 + M_1\kappa_1 + M_2\kappa_2,$$

$$b_2 = e^{\lambda}\beta\lambda(M_1+M_2)[D_1(\kappa_1\eta_1^2+\alpha_1) + D_2(\kappa_2\eta_2^2+\alpha_2)],$$

$$b_4 = \frac{1}{4}(-[e^{\lambda}\beta\Delta^2\lambda\kappa_1\eta_1^2 + 4\eta_2^2\kappa_1\kappa_2\eta_1^2 + \alpha_2(e^{\lambda}\beta\lambda\Delta^2 + 4\eta_1^2\kappa_1) + e^{\lambda}\beta\Delta^2\lambda\eta_2^2\kappa_2 + \alpha_1(e^{\lambda}\beta\lambda\Delta^2 + 4\alpha_2 + 4\eta_2^2\kappa_2)]D_{12}^2 - 4e^{\lambda}\beta\Delta\lambda(M_1\eta_1\kappa_1 - M_2\eta_2\kappa_2)D_{12} + 4e^{\lambda}\beta\lambda\{M_1M_2(\kappa_1+\kappa_2) + D_2[M_1\gamma_2 + M_2(\gamma_2+\Delta\eta_2\kappa_2)]\} + D_1\{4e^{\lambda}\beta\lambda[M_2\gamma_1 + M_1(\gamma_1-\Delta\eta_1\kappa_1)] + D_2[e^{\lambda}\beta\Delta^2\lambda\kappa_1\eta_1^2 + 4\eta_2^2\kappa_1\kappa_2\eta_1^2 + \alpha_2(e^{\lambda}\beta\lambda\Delta^2 + 4\eta_1^2\kappa_1) + e^{\lambda}\beta\Delta^2\lambda\eta_2^2\kappa_2 + \alpha_1(e^{\lambda}\beta\lambda\Delta^2 + 4\alpha_2 + 4\eta_2^2\kappa_2)]\} + D_1\{4e^{\lambda}\beta\lambda[M_2\gamma_1 + M_1(\gamma_1-\Delta\eta_1\kappa_1)] + D_2[e^{\lambda}\beta\Delta^2\lambda\kappa_1\eta_1^2 + 4\eta_2^2\kappa_1\kappa_2\eta_1^2 + \alpha_2(e^{\lambda}\beta\lambda\Delta^2 + 4\eta_1^2\kappa_1) + e^{\lambda}\beta\Delta^2\lambda\eta_2^2\kappa_2 + \alpha_1(e^{\lambda}\beta\lambda\Delta^2 + 4\alpha_2 + 4\eta_2^2\kappa_2)]\}),$$

$$b_6 = \frac{1}{4}(2e^{\lambda}\beta\lambda D_{12}(M_1\kappa_1 + M_2\kappa_2)\Delta^2 - D_{12}^2[\gamma_2(e^{\lambda}\beta\lambda\Delta^2 + 4\alpha_1 + 4\eta_1^2\kappa_1) + \gamma_1(e^{\lambda}\beta\lambda\Delta^2 + 4\alpha_2 + 4\eta_2^2\kappa_2)] + D_2[M_2(e^{\lambda}\beta\lambda\Delta^2 + 4\alpha_2)\kappa_2 + M_1\kappa_1(e^{\lambda}\beta\lambda\Delta^2 + 4\alpha_2 + 4\eta_2^2\kappa_2)] + D_1\{M_1(e^{\lambda}\beta\lambda\Delta^2 + 4\alpha_1)\kappa_1 + M_2(e^{\lambda}\beta\lambda\Delta^2 + 4\alpha_1 + 4\eta_1^2\kappa_1)\kappa_2 + D_2[\gamma_2(e^{\lambda}\beta\lambda\Delta^2 + 4\alpha_1 + 4\eta_1^2\kappa_1) + \gamma_1(e^{\lambda}\beta\lambda\Delta^2 + 4\alpha_2 + 4\eta_2^2\kappa_2)]\}),$$

$$b_8 = -\gamma_1\gamma_2 D_{12}^2 + D_2 M_1 \gamma_2 \kappa_1 + D_2 M_2 \gamma_2 \kappa_2 + M_1 M_2 \kappa_1 \kappa_2 + D_1 \gamma_1 (D_2 \gamma_2 + M_1 \kappa_1 + M_2 \kappa_2),$$

$$c_4 = e^{\lambda}\beta\lambda (D_1 D_2 - D_{12}^2)(M_1 + M_2)(\kappa_1 \eta_1^2 + \alpha_1)(\kappa_2 \eta_2^2 + \alpha_2),$$

$$c_6 = e^{\lambda}\beta\lambda[-\{M_1[\gamma_2 \kappa_1 \eta_1^2 - \Delta \eta_2^2 \kappa_1 \kappa_2 \eta_1 + \alpha_1 \gamma_2 + \alpha_2(\gamma_1 - \Delta \eta_1 \kappa_1) + \gamma_1 \eta_2^2 \kappa_2] + M_2[\gamma_2 \kappa_1 \eta_1^2 + \Delta \eta_2 \kappa_1 \kappa_2 \eta_1^2 + \alpha_2 \gamma_1 + \gamma_1 \eta_2^2 \kappa_2 + \alpha_1(\gamma_2 + \Delta \eta_2 \kappa_2)]\} D_{12}^2 - 2 M_1 M_2 \eta_1 \eta_2 \kappa_1 \kappa_2 D_{12} + D_2 M_1 M_2[\kappa_1 \kappa_2 \eta_2^2 + \alpha_2(\kappa_1 + \kappa_2)] + D_1(M_1 M_2[\kappa_1 \kappa_2 \eta_1^2 + \alpha_1(\kappa_1 + \kappa_2)] + D_2\{M_1(\gamma_2 \kappa_1 \eta_1^2 - \Delta \eta_2^2 \kappa_1 \kappa_2 \eta_1 + \alpha_1 \gamma_2 + \alpha_2(\gamma_1 - \Delta \eta_1 \kappa_1) + \gamma_1 \eta_2^2 \kappa_2 + M_2[\gamma_2 \kappa_1 \eta_1^2 + \Delta \eta_2 \kappa_1 \kappa_2 \eta_1^2 + \alpha_2 \gamma_1 + \gamma_1 \eta_2^2 \kappa_2 + \alpha_1(\gamma_2 + \Delta \eta_2 \kappa_2)]\})],$$

$$c_8 = \frac{1}{4}(-\{M_2\{[e^{\lambda}\beta\Delta^2\lambda \kappa_1 \eta_1^2 + \alpha_1(e^{\lambda}\beta\lambda\Delta^2 + 4\alpha_2) + \alpha_2(e^{\lambda}\beta\lambda\Delta^2 + 4\eta_1^2\kappa_1)]\kappa_2 + 4e^{\lambda}\beta\lambda\gamma_1(\gamma_2 + \Delta\eta_2\kappa_2)\} + M_1\{4e^{\lambda}\beta\lambda\gamma_1\gamma_2 + \kappa_1[\alpha_1(e^{\lambda}\beta\lambda\Delta^2 + 4\alpha_2 + 4\eta_2^2\kappa_2) + e^{\lambda}\beta\Delta\lambda(\Delta\kappa_2\eta_2^2 + \Delta\alpha_2 - 4\gamma_2\eta_1)]\} D_{12}^2 - 4e^{\lambda}\beta\Delta\lambda M_1 M_2(\eta_1 - \eta_2)\kappa_1\kappa_2 D_{12} + 4e^{\lambda}\beta\lambda D_2 M_1 M_2[\Delta\eta_2\kappa_1\kappa_2 + \gamma_2(\kappa_1 + \kappa_2)] + D_1[4e^{\lambda}\beta\lambda M_1 M_2[\gamma_1(\kappa_1 + \kappa_2) - \Delta\eta_1\kappa_1\kappa_2] + D_2(M_2\{[e^{\lambda}\beta\Delta^2\lambda\kappa_1\eta_1^2 + \alpha_1(e^{\lambda}\beta\lambda\Delta^2 + 4\alpha_2) + \alpha_2(e^{\lambda}\beta\lambda\Delta^2 + 4\eta_1^2\kappa_1)]\kappa_2 + 4e^{\lambda}\beta\lambda\gamma_1(\gamma_2 + \Delta\eta_{2\kappa_2})\} + M_1\{4e^{\lambda}\beta\lambda\gamma_1\gamma_2 + \kappa_1[\alpha_1(e^{\lambda}\beta\lambda\Delta^2 + 4\alpha_2 + 4\eta_2^2\kappa_2) + e^{\lambda}\beta\Delta\lambda(\Delta\kappa_2\eta_2^2 + \Delta\alpha_2 - 4\gamma_2\eta_1)]\})]\}),$$

$$c_{10} = \frac{1}{4}(2e^{\lambda}\beta\lambda D_{12} M_1 M_2 \kappa_1 \kappa_2 \Delta^2 + D_2 M_1 M_2(e^{\lambda}\beta\lambda\Delta^2 + 4\alpha_2)\kappa_1\kappa_2 - D_{12}^2\{M_2[(e^{\lambda}\beta\lambda\Delta^2 + 4\alpha_2)\gamma_1 + \gamma_2(e^{\lambda}\beta\lambda\Delta^2 + 4\alpha_1 + 4\eta_1^2\kappa_1)]\kappa_2 + M_1\kappa_1[(e^{\lambda}\beta\lambda\Delta^2 + 4\alpha_1)\gamma_2 + \gamma_1(e^{\lambda}\beta\lambda\Delta^2 + 4\alpha_2 + 4\eta_2^2\kappa_2)]\} + D_1[M_1 M_2(e^{\lambda}\beta\lambda\Delta^2 + 4\alpha_1)\kappa_1\kappa_2 + D_2(M_2\{(e^{\lambda}\beta\lambda\Delta^2 + 4\alpha_2)\gamma_1 + \gamma_2(e^{\lambda}\beta\lambda\Delta^2 + 4\alpha_1 + 4\eta_1^2\kappa_1)\kappa_2 + M_1\kappa_1[(e^{\lambda}\beta\lambda\Delta^2 + 4\alpha_1)\gamma_2 + \gamma_1(e^{\lambda}\beta\lambda\Delta^2 + 4\alpha_2 + 4\eta_2^2\kappa_2)]\})]),$$

$$c_{12} = D_1\gamma_1[M_1 M_2 \kappa_1\kappa_2 + D_2\gamma_2(M_1\kappa_1 + M_2\kappa_2)] - \gamma_2[D_{12}^2\gamma_1(M_1\kappa_1 + M_2\kappa_2) - D_2 M_1 M_2 \kappa_1\kappa_2],$$

$$d_8 = e^{\lambda}\beta\lambda(D_1 D_2 - D_{12}^2) M_1 M_2\{\alpha_2\kappa_1\kappa_2\eta_1^2 + \alpha_1[\kappa_1\kappa_2\eta_2^2 + \alpha_2(\kappa_1 + \kappa_2)]\},$$

$$d_{10} = e^{\lambda}\beta\lambda(D_1 D_2 - D_{12}^2) M_1 M_2\{(\gamma_2\eta_1^2 + \gamma_1\eta_2^2)\kappa_1\kappa_2 + \alpha_2[\gamma_1(\kappa_1 + \kappa_2) - \Delta\eta_1\kappa_1\kappa_2] + \alpha_1[\Delta\eta_2\kappa_1\kappa_2 + \gamma_2(\kappa_1 + \kappa_2)]\},$$

$$d_{12} = \frac{1}{4}(D_1 D_2 - D_{12}^2) M_1 M_2\{[\alpha_1(e^{\lambda}\beta\lambda\Delta^2 + 4\alpha_2) + e^{\lambda}\beta\Delta\lambda(\Delta\alpha_2 - 4\gamma_2\eta_1)]\kappa_1\kappa_2 + 4e^{\lambda}\beta\lambda\gamma_1[\Delta\eta_2\kappa_1\kappa_2 + \gamma_2(\kappa_1 + \kappa_2)]\},$$

$$d_{14} = \frac{1}{4}(D_1 D_2 - D_{12}^2) M_1 M_2[(e^{\lambda}\beta\lambda\Delta^2 + 4\alpha_2)\gamma_1 + (e^{\lambda}\beta\lambda\Delta^2 + 4\alpha_1)\gamma_2]\kappa_1\kappa_2,$$

$$d_{16} = (D_1 D_2 - D_{12}^2) M_1 M_2 \gamma_1\gamma_2\kappa_1\kappa_2.$$

[1] B. Alberts *et al.*, *The Cell* (Garland Science, New York, 2002).
[2] R. Lipowsky and E. Sackmann, *Structure and Dynamics of Membranes* (Elsevier, Amsterdam, 1995).
[3] R. Lipowsky, Nature (London) **349**, 475 (1991).
[4] S. J. Singer and G. L. Nicolson, Science **175**, 720 (1972).
[5] D. Nelson, T. Piran, and S. Weinberg, *Statistical Mechanics of Membranes and Surfaces* (World Scientific, New York, 1989).
[6] P. B. S. Kumar, G. Gompper, and R. Lipowsky, Phys. Rev. E **60**, 4610 (1999).
[7] W. T. Gozdz and G. Gompper, Phys. Rev. E **59**, 4305 (1999).
[8] T. Taniguchi, Phys. Rev. Lett. **76**, 4444 (1996).
[9] P. B. S. Kumar and M. Rao, Phys. Rev. Lett. **80**, 2489 (1998).
[10] P. B. S. Kumar, G. Gompper, and R. Lipowsky, Phys. Rev. Lett. **86**, 3911 (2001).
[11] F. Julicher and R. Lipowsky, Phys. Rev. Lett. **70**, 2964 (1993).
[12] R. Lipowsky, Curr. Opin. Struct. Biol. **5**, 531 (1995).
[13] L. Li, X. Liang, M. Lin, F. Qiu, and Y. Yang, J. Am. Chem. Soc. **127**, 2489 (1998).
[14] R. Lipowsky, J. Phys. II **2**, 1825 (1992).
[15] F. Julicher and R. Lipowsky, Phys. Rev. Lett. **70**, 2964 (1993).
[16] J. Prost and R. Bruinsma, Europhys. Lett. **33**, 321 (1996).
[17] S. Ramaswamy, J. Toner, and J. Prost, Phys. Rev. Lett. **84**, 3494 (2000).
[18] H.-Y. Chen, Phys. Rev. Lett. **92**, 168101 (2004).
[19] S. Sankararaman, G. I. Menon, and P. B. Sunil Kumar, Phys. Rev. E **66**, 031914 (2002).
[20] J. B. Manneville, P. Bassereau, S. Ramaswamy, and J. Prost, Phys. Rev. E **64**, 021908 (2001).
[21] R. Reigada, J. Buceta, and K. Lindenberg, Phys. Rev. E **71**, 051906 (2005).
[22] R. Reigada, J. Buceta, and K. Lindenberg, Phys. Rev. E **72**, 051921 (2005).
[23] E. I. Kats, V. V. Lebedev, and S. V. Malinin, JETP **86**, 1149 (1998).
[24] M. Spivak, *A Comprehensive Introduction to Differential Geometry* (Publish or Perish, Houston, 1975), Vols. 3 and 5.

[25] W. Helfrich, Z. Naturforsch. C **28**, 693 (1973).
[26] O. Kuksenok and A. C. Balazs, Phys. Rev. E **75**, 051906 (2007).
[27] C. M. Funkhouser, F. J. Solis, and K. Thornton, Phys. Rev. E **76**, 011912 (2007).
[28] H. J. Kreuzer, *NonequilibriumThermodynamics and Its Statistical Foundations* (Oxford University Press, Oxford, 1983).
[29] F. R. Gantmacher, *Applications of the Theory of Matrices*, translated by J. L. Brenner *et al.* (Interscience, New York, 1959).
[30] D. Walgraef, *Spatio-Temporal Pattern Formation: With Examples from Physics, Chemistry, and Materials Science* (Springer, New York, 1997).